Journal of Zhejiang University-SCIENCE B 2025 26(9):881-896
www.jzus.zju.edu.cn; www.springer.com/journal/11585
E-mail: jzus_b@zju.edu.cn

Research Article
https://doi.org/10.1631/jzus.B2400203

Check for updates

NRF2 nuclear translocation and interaction with DUSP1 regulate the osteogenic differentiation of murine mandibular osteoblasts stimulated with *Porphyromonas gingivalis* lipopolysaccharide

Xufei YU[1,2*], Jiaqi BAO[1*], Yingming WEI[1*], Yuting YANG[1], Wenlin YUAN[1], Lili CHEN[1✉], Zhongxiu WANG[1✉]

[1]*Department of Periodontology, The Second Affiliated Hospital, School of Medicine, Zhejiang University, Hangzhou 310009, China*
[2]*Cancer Institute, The Second Affiliated Hospital, School of Medicine, Zhejiang University, Hangzhou 310009, China*

Abstract: Background: Periodontitis is characterized by alveolar bone resorption, aggravated by osteoblast dysfunction, and associated with intracellular oxidative stress linked to the nuclear factor erythroid 2-related factor 2 (NRF2) level. We evaluated the molecular mechanism of periodontitis onset and development and the role of NRF2 in osteogenic differentiation. Methods: Primary murine mandibular osteoblasts were extracted and exposed to *Porphyromonas gingivalis* lipopolysaccharide (*Pg*-LPS) or other stimuli. Reactive oxygen species (ROS) and 5,5',6,6'-tetrachloro-1,1',3,3'-tetraethylbenzimidazolylcarbocyanine iodide (JC-1) staining were used to detect intracellular oxidative stress. Alkaline phosphatase staining and alizarin red S staining were used to detect the osteogenic differentiation of osteoblasts. Immunofluorescence and western blotting were used to determine the changes in the mitogen-activated protein kinase (MAPK) pathway and related molecule activities. Immunofluorescence colocalization and co-immunoprecipitation were performed to examine the nuclear translocation of NRF2 and its interaction with dual-specific phosphatase 1 (DUSP1) in cells. Results: Ligated tissue samples showed higher alveolar bone resorption rate and lower NRF2 level than healthy periodontal tissue samples. *Pg*-LPS increased intracellular oxidative stress levels and inhibited osteogenic differentiation, whereas changes in NRF2 expression were correlated with changes in the oxidative stress and osteogenesis rate. NRF2 promoted the dephosphorylation of the MAPK pathway by nuclear translocation and the upregulation of DUSP1 expression, thus enhancing the osteogenic differentiation capacity of mandibular osteoblasts. The interaction between NRF2 and DUSP1 was observed. Conclusions: NRF2 and its nuclear translocation can regulate the osteogenic differentiation of mandibular osteoblasts under *Pg*-LPS conditions by interacting with DUSP1 in a process linked to the MAPK pathway. These findings form the basis of periodontitis treatment.

Key words: Periodontitis; Nuclear factor erythroid 2-related factor 2 (NRF2); Dual-specific phosphatase 1 (DUSP1); Mitogen-activated protein kinase (MAPK); Oxidative stress; Osteogenesis

1 Introduction

Periodontitis is a chronic infectious disease characterized by alveolar bone resorption (Loos and van Dyke, 2020). Lipopolysaccharide (LPS) is crucial in the pathogenesis of periodontitis and inflammatory bone resorption (Fiedler et al., 2013). *Porphyromonas gingivalis* LPS (*Pg*-LPS) could promote the production of pro-inflammatory cytokines (Herzmann et al., 2017), accelerating alveolar bone destruction. Alveolar bone homeostasis is maintained via a dynamic balance between osteoclast-mediated bone resorption and osteoblast-mediated bone formation (Kim et al., 2020). However, further research is needed to delve into the underlying mechanisms by which *Pg*-LPS disrupts bone balance, leading to the continuous destruction of alveolar bone in periodontitis.

An imbalance between the oxidative and antioxidant systems causes oxidative stress, as it involves the accumulation of free radicals and reactive oxygen

✉ Zhongxiu WANG, 21518119@zju.edu.cn
Lili CHEN, chenlili_1030@zju.edu.cn
* The three authors contributed equally to this work
Zhongxiu WANG, https://orcid.org/0000-0001-8498-2678
Lili CHEN, https://orcid.org/0000-0002-0620-8844
Xufei YU, https://orcid.org/0009-0009-7989-8637
Jiaqi BAO, https://orcid.org/0000-0001-5265-8064
Yingming WEI, https://orcid.org/0000-0003-1638-3707

Received Apr. 22, 2024; Revision accepted Aug. 10, 2024; Crosschecked Sept. 16, 2025

species (ROS), disrupting nucleic acid, protein, and lipid functions in the cell (Sies et al., 2017). The levels of oxidative stress markers, such as ROS and malondialdehyde, are increased in saliva (Su et al., 2009) and gingival tissue samples (Konopka et al., 2007) collected from patients with periodontitis. The ROS content increases in human gingival fibroblasts (HGFs) and human periodontal ligament cells (hPDLCs) upon the stimulation with *Pg*-LPS and tumor necrosis factor-α (TNF-α) (Fang et al., 2020; Liu et al., 2023). This suggests a correlation between periodontitis and oxidative stress, which may be bi-directional.

Nuclear factor erythroid 2-related factor 2 (NRF2), encoded by *NFE2L2*, protects cells from oxidative stress. Oxidative stress causes the dissociation of NRF2 and kelch-like ECH-associated protein 1 (KEAP1), triggering the nuclear transfer of NRF2 (Baird et al., 2014). Active cytoplasmic proteins are transported into the nucleus to influence cell functions in a process called nuclear translocation (Knudsen et al., 2009). Because NRF2 and its nuclear translocation regulate the cellular responses against potentially harmful levels of oxidative stress, they are termed redox molecular switches (Silva-Islas and Maldonado, 2018; Wang L et al., 2022). Zhu et al. (2020) utilized LPS to stimulate human gingival epithelial cells (hGECs) and found that the fluorescence intensity of nuclear translocation of NRF2 decreased, while the levels of NRF2-target antioxidant genes, catalase (*CAT*), γ-glutamylcysteine synthetase, heavy subunit (*GCLC*), and superoxide dismutase 1 (*SOD1*), were significantly reduced, coupled with an elevation in the ROS level, suggesting the role of redox molecular switches in the development of periodontitis.

Sun et al. (2015) reported that *Nfe2l2*-knockout mice had low bone mass due to reduced bone formation, while the activation of NRF2 by natural products improved osteoporosis in rats (Liu et al., 2018; Tang et al., 2020). Osteoblast differentiation requires the activation of SOD2 to eliminate accumulated ROS (Chen et al., 2008), whereas NRF2 plays a regulatory role in antioxidation and promotes the transformation of mesenchymal stem cells (MSCs) into osteoblasts (Yen et al., 2020). However, whether NRF2 and its nuclear translocation influence *Pg*-LPS-induced osteogenic differentiation remains unclear.

Under various extracellular stimuli, the mitogen-activated protein kinase (MAPK) family of protein kinases functions as key signal transducers (Kim et al., 2019). Fu et al. (2019) revealed that dual-specific phosphatase 1 (DUSP1), a crucial signaling molecule in the cascade reaction of the MAPK signaling pathway, could inactivate c-Jun N-terminal kinase (JNK), p38, extracellular signal-regulated kinase (ERK), and other signaling molecules via interactions with dephosphorylation of the MAPK protein family, which regulated the core mediators of osteoblast differentiation (Greenblatt et al., 2010; Wu et al., 2016; Zhu et al., 2019). *DUSP1* encodes mitogen-activated protein kinase phosphatase-1 (MKP-1), which is often interchangeable with DUSP1. Chung et al. (2014) reported that during the process of differentiating hPDLCs into osteoblasts, changes in the phosphorylation levels of p38 MAPK and ERK were observed in osteoblasts upon the downregulation of *NRF2* gene expression or the oxidative stress inhibitor *N*-acetylcysteine (NAC). Furthermore, alkaline phosphatase (ALP) and osteocalcin (OCN) levels were decreased. Recently, Xiao et al. (2023) found that an increase in MAPK phosphorylation accompanies Runt-related transcription factor 2 (RUNX2) and OCN inhibition, and that osteoblast markers are elevated following the application of officinalis to reduce MAPK phosphorylation.

We investigated the role of NRF2 and its nuclear translocation in the regulation of the differentiation ability of mandibular osteoblasts via the MAPK pathway and explored the relationship between the antioxidant molecular switch NRF2 and the key signaling molecule DUSP1 of the MAPK pathway. The study findings may help elucidate the molecular mechanism of periodontitis onset and development as well as explore the key molecules involved in oxidative stress in the *Pg*-LPS-stimulated microenvironment.

2 Materials and methods

2.1 Experimental periodontitis animal model

Six-week-old male pathogen-free C57BL/6 mice (China Experimental Animal Center, Hangzhou, China) were randomly divided into two groups. One group was left untreated (the control group), and the other group (the periodontitis group) was fixed with 5-0 silk around the bilateral maxillary second molars for 7 d to establish an experimental periodontitis model (Abe and Hajishengallis, 2013). The gingiva of the periodontitis

group was injected with 100 μg/mL *Pg*-LPS (InvivoGen, San Diego, California, USA) every 2 d for one week, and ligation was checked to prevent the breaking of the ligated silk during the experiment.

After the mice were euthanized by cervical dislocation, murine maxillae were separated. Micro-computed tomography (micro-CT; U-CT-XUHR, the Netherlands) was used to capture the maxillae and reconstruct three-dimensional (3D) images.

2.2 Histopathology and immunohistochemistry

Five different samples were collected from both healthy individuals and patients with periodontitis. The alveolar bone and gingival tissue samples were fixed in 4% (0.04 g/mL) paraformaldehyde for 48 h. The alveolar bone samples were decalcified in ethylenediaminetetraacetic acid (EDTA) (Servicebio, Wuhan, China) for two weeks. Tissue samples were cut into sections and treated with hematoxylin-eosin (HE) or immunohistochemical (IHC) staining. IHC findings were quantitatively evaluated using the ImageJ software (National Institutes of Health, Bethesda, MD, USA).

2.3 Cell culture

Mandibular osteoblasts were derived from 1-d-old C57BL/6 mice (China Experimental Animal Center). After the mice were euthanized, their mandibles were removed, washed with sterile phosphate-buffered saline (PBS; Servicebio), and cut into fragments. The fragments were cultured with high-glucose Dulbecco's modified Eagle's medium (DEME; Gibco, Grand Island, NY, USA) supplemented with 10% (volume fraction) fetal bovine serum (FBS; Gibco) in culture flasks. Osteoblasts from passages 2 and 3 were used for further experiments. Osteogenic induction included a control medium supplemented with 50 μg/mL L-ascorbic acid, 10 nmol/L dexamethasone, and 10 mmol/L β-glycerophosphate (Sigma, St. Louis, MO, MA, USA). To prepare various concentrations of LPS, 1 mg of standard *Pg*-LPS was dissolved in 1 mL of endotoxin-free water and filtered through a needle filter. All the cells were cultured at 37 °C with 5% CO_2.

2.4 Cell viability assay

We used cell counting kit-8 (CCK-8; Boster, Wuhan, China) to detect the effects of *Pg*-LPS (0, 0.1, 0.2, 0.5, 1.0, 2.0, 5.0, and 10.0 μg/mL; InvivoGen) on the viability of mandibular osteoblasts. Osteoblasts were seeded in 96-well plates and incubated for 1, 3, or 7 d. After the cells were cultured for a predetermined time, 10 μL of CCK-8 solution was added to each well and incubated in the dark at 37 °C with 5% CO_2 for 60 min. The optical density at 450 nm was measured using a spectrophotometer (Bio-Rad, CA, USA).

2.5 Alkaline phosphatase staining

Mandibular osteoblasts were seeded into 24-well plates at the same cell density. When the cells reached 80% confluence, the DMEM was replaced with osteogenic inducers, and the cells were exposed to *Pg*-LPS (0.1, 0.5, or 1.0 μg/mL) for 3, 5, and 7 d, or cultured by 1.0 μg/mL *Pg*-LPS with 50 nmol/L brusatol or 10 μmol/L tert-butylhydroquinone (TBHQ) (Selleck Chemicals, Houston, TX, USA) for 5 d.

Subsequently, cells were fixed with paraformaldehyde for 30 min, and the 5-bromo-4-chloro-3-indolyl phosphate/nitroblue tetrazolium (BCIP/NBT) Kit (Beyotime, Shanghai, China) was used for ALP staining, which was carried out for 4 h. Stained images were recorded under a light microscope (Leica, Wetzlar, Germany).

2.6 Alizarin red S staining

Mandibular osteoblasts were seeded into 48-well plates and treated with an osteogenic induction medium supplemented with *Pg*-LPS, brusatol, or TBHQ. After incubation for 21 d, mandibular osteoblasts were fixed with paraformaldehyde for 30 min and stained with the Alizarin Red S Staining Kit (Beyotime) for osteogenesis at 37 °C for 30 min. Once captured, the mineralized nodules were quantified using 100 mmol/L cetylpyridinium chloride solution (Sigma), and the absorbance at 562 nm was measured using a spectrophotometer.

2.7 RNA sequencing

Osteoblasts were treated with 1.0 μg/mL *Pg*-LPS for 3 d followed by whole-transcriptome sequencing. Total RNA was collected using TRIzol (Invitrogen, Carlsbad, CA, USA). Three different samples were collected from both the LPS and control groups. Sequencing was performed (LC-Bio Technologies Co., Ltd., Hangzhou, China) using the Illumina NovaSeq™ 6000 platform (Illumina, San Diego, CA, USA) following standard procedures.

Utilizing Cutadapt, we filtered unqualified sequences from the raw data to obtain clean data. Then, HISAT2 was used for reference genome comparison,

transcripts were reconstructed, and gene expression levels in each sample were quantified using Stringtie based on HISAT2 results.

2.8 ROS detection

The intracellular ROS levels were assessed using the ROS Assay Kit (Beyotime). Cells were seeded in 24-well plates and exposed to *Pg*-LPS for 24 h. Following the treatment, the cells were incubated with 2',7'-dichlorodihydrofluorescein-diacetate (DCFH-DA) at 37 ℃ for 20 min and subsequently observed under a fluorescence microscope (Zeiss, Oberkochen, Germany). Intracellular ROS can oxidize non-fluorescent DCFH to produce fluorescent dichlorofluorescein (DCF). Thus, DCF fluorescence can reflect the intracellular ROS level.

2.9 Mitochondrial membrane potential measurement

Mitochondrial membrane potential (MMP) was determined using the MMP Assay Kit with 5,5',6,6'-tetrachloro-1,1',3,3'-tetraethylbenzimidazolylcarbocyanine iodide (JC-1; Beyotime). Briefly, treated cells were mixed with equal amounts of JC-1 staining solution and cell culture medium. The cells were incubated at 37 ℃ for 20 min. MMP can be expressed as the ratio of red-to-green fluorescence intensity.

2.10 Quantitative real-time polymerase chain reaction

Total RNA was extracted using the TRIzol reagent. Reverse transcription was performed using the Hifair® II 1st Strand cDNA Synthesis Kit (Yeasen, Shanghai, China). The levels of the target genes were detected using the SYBR Green Master Mix Kit (Yeasen) with the ABI 7500 Fast real-time polymerase chain reaction (PCR) system (Applied Biosystems, Foster City, CA, USA). Each messenger RNA (mRNA) was normalized to the glyceraldehyde-3-phosphate dehydrogenase (GAPDH) level, and the relative mRNA expression was calculated using the $2^{-\Delta\Delta C_T}$ method. The primer sequences are listed in Table S1.

2.11 Cell fractionation

Nuclear and cytoplasmic proteins were extracted from mandibular osteoblasts using cytoplasmic and nuclear protein extraction kits (Beyotime). Cytoplasmic protein extraction reagents A and B were added, and after centrifugation, the absorbed supernatant was the extracted cytoplasmic protein. The nuclear proteins were extracted using a nuclear protein extraction reagent according to the specification.

2.12 Western blotting

Total proteins from cells or tissues were extracted using the M-PER™ mammalian protein extraction reagent (Thermo Fisher Scientific, Waltham, MA, USA) supplemented with protein inhibitors (Fdbio Science, Shanghai, China). Proteins were separated by sodium dodecyl sulfate-polyacrylamide gel electrophoresis (SDS-PAGE) and transferred onto polyvinylidene fluoride membranes (Bio-Rad). The membranes were blocked with 5% (0.05 g/mL) skim milk for 1 h, and subsequently incubated with primary antibodies (Table S2) at 4 ℃ overnight.

After incubation, the membranes were further incubated with the appropriate secondary antibodies for 1 h. Protein bands were visualized using an enhanced chemiluminescence (ECL) kit (Fdbio Science) with a chemiluminescent imaging system (Tanon, Shanghai, China) and were analyzed.

2.13 Immunofluorescence staining

After being cultured with 1.0 μg/mL LPS or 10 μmol/L TBHQ, osteoblasts were immobilized in 4% (0.04 g/mL) formaldehyde for 30 min. The cells were permeabilized with 0.3% (volume fraction) Triton X-100 for 5 min. After being blocked for 1 h with 5% (0.05 g/mL) bovine serum albumin (BSA; Sangon Biotech, Shanghai, China), the cells were treated with anti-NRF2 (Affinity, Cincinnati, OH, USA; AF0639)/anti-DUSP1 (Santa Cruz Biotechnology, USA; sc-373841) antibodies at 4 ℃ overnight. The cells were subsequently treated with iFluor™ 488/594 secondary antibodies (HUABIO, Hangzhou, China; HA1121, HA1122) and incubated in a dark room at 25 ℃ for 1 h. The cells were stained with 4',6-diamidino-2-phenylindole (DAPI; Biosharp, Shanghai, China) for 10 min and imaged using a confocal fluorescence microscope.

2.14 *NRF2* small interfering RNA/*NRF2*-overexpressed plasmid transient transfection

Mandibular osteoblasts were cultured in 6-well plates until the cell density reached 80%. Transient transfections with *NRF2* small interfering RNA (siRNA; GenePharma, Suzhou, China) and *NRF2*-overexpressed plasmids (Leqi, Hangzhou, China) were performed using the Lipo6000™ transfection reagent (Beyotime).

After transfection at 37 ℃ for 6 h, the culture medium was replaced with an osteogenic induction solution containing 1.0 μg/mL LPS for 72 h, and the knockout and overexpression effects were analyzed using western blotting. The following *NRF2* siRNA sequences were used in the experiments: sense, 5'-AGACAUAGAUC UUGGAGUATT-3'; and anti-sense: 5'-UACUCCAAG AUCUAUGUCUTT-3'.

2.15 Co-immunoprecipitation

Co-immunoprecipitation (Co-IP) was performed to validate protein–protein interactions. Mandibular osteoblasts from different groups were lysed using a protein A/G immunoprecipitation kit (Solarbio, Beijing, China). The rinsed magnetic beads were mixed with 5 μg of an antibody and incubated at room temperature for 30 min. The magnetic beads were washed and incubated with cell-lysed samples overnight at 4 ℃. The immunocomplexes were washed thrice with IP washing buffer, and the bound proteins were eluted by boiling loading buffer. Equal quantities of proteins were obtained for western blot analysis. The names and catalog numbers of the reagents used above are listed in Table S3.

2.16 Statistical analysis

The results are expressed as mean±standard deviation (SD) of at least three replicates. One-way analysis of variance (ANOVA) and Student's *t*-test were used to compare the differences between groups using GraphPad Prism 8.4.0 (San Diego, CA, USA). Significance was set at $P<0.05$.

3 Results

3.1 Expression of NRF2 in alveolar bone and gingival tissue

After 7 d, 3D reconstruction revealed that bone absorption was more severe in the periodontitis ligation group than in the control group (Fig. 1a). After ligation, HE staining showed more substantial inflammatory cell infiltration in the periodontal tissues of the maxillary second molars in the periodontitis group compared to that in the control group (Figs. 1b and 1d). IHC staining and quantitative evaluation revealed that NRF2 expression significantly decreased after ligation in the murine maxillary specimens (Figs. 1c and 1e). The expression of NRF2 in the milled tissue of the murine maxilla was observed by western blotting after lysis buffer treatment. NRF2 expression was reduced in the periodontitis group (Figs. 1f and 1g).

Furthermore, IHC staining showed that NRF2 expression in the alveolar bone and gingival tissues was lower in the periodontitis group than in healthy controls (Fig. 1h). ImageJ analysis confirmed the decrease in NRF2 levels in the periodontitis group (Figs. 1i and 1j).

3.2 Effects of *Pg*-LPS on osteogenic differentiation

CCK-8 was used to determine cell viability after LPS treatment over time (Figs. 2a–2c). Cell viability was comparable among the groups after 1, 3, or 7 d of treatment. No cytotoxic effect of LPS was observed.

Quantitative reverse transcription PCR (RT-qPCR) results after 2 and 5 d (Figs. 2d–2i) and western blotting results after 3 d (Figs. 2j and 2k) confirmed the LPS concentration-dependent downregulation of osteogenic genes at the mRNA and protein levels.

ALP staining showed that LPS reduced ALP activity and inhibited osteoblast differentiation in a dose-dependent manner at 3, 5, and 7 d (Figs. 2l–2q). After 21 d, alizarin red staining and quantitative analysis showed that LPS inhibited the formation of mineralized nodules (Figs. 2r and 2s), further confirming the inhibition of osteoblast calcification.

3.3 Influence of *Pg*-LPS on oxidative stress

Sequencing identified 62 differentially expressed genes (45 upregulated, 17 downregulated) (Figs. 3a and 3b). Gene Ontology (GO) enrichment analysis revealed differences in the biological process-related genes related to ROS production (Figs. 3c and 3d).

ROS staining revealed intracellular ROS levels (Figs. 3e and 3f). Compared with the control group (osteogenic induction), the fluorescence intensity of the cells after 24 h of treatment increased with increasing concentrations of LPS (0.1, 0.5, and 1.0 μg/mL). We examined MMP in osteoblasts treated with LPS using JC-1 staining (Figs. 3g–3j). With increasing LPS concentration, the red fluorescence intensity gradually decreased, while the green fluorescence gradually increased.

3.4 Inhibition of NRF2 expression and nuclear translocation by *Pg*-LPS

The expression and distribution of NRF2 protein in mandibular osteoblasts were observed by immunofluorescence staining (Figs. 3k–3p). The fluorescence

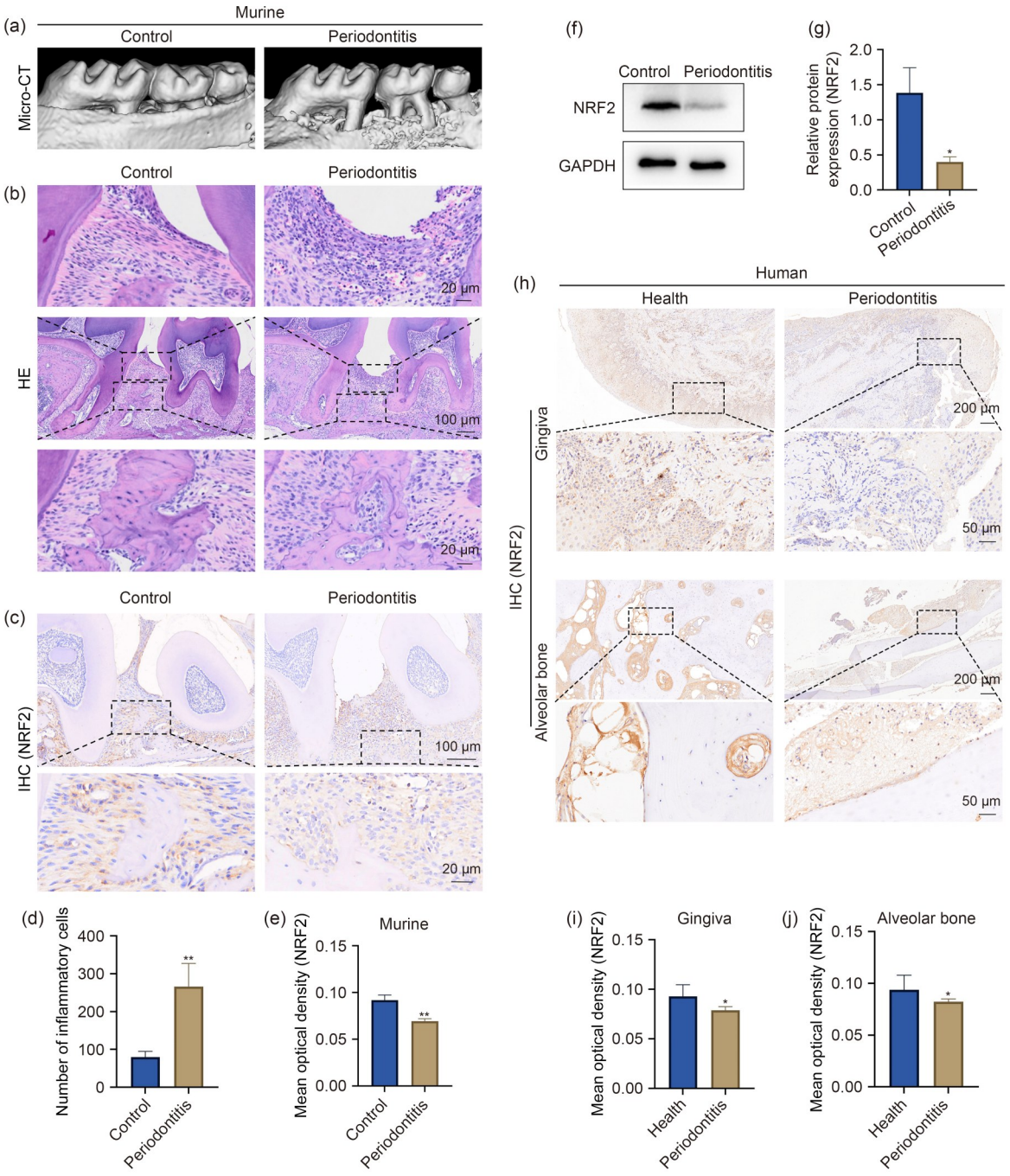

Fig. 1 NRF2 expression in alveolar bone and gingival tissue samples. (a) Micro-computed tomography (micro-CT) with three-dimensional (3D) reconstructed images of the maxillae. (b, d) Hematoxylin-eosin (HE) staining and quantification of inflammatory cells in periodontal tissues. (c, e) Immunohistochemical (IHC) staining and quantification of NRF2 in the maxilla. (f, g) Western blot and quantification of NRF2 in the maxilla. (h–j) IHC staining and mean optical density of NRF2 in gingival tissue samples and alveolar bone samples. * $P<0.05$, ** $P<0.01$ vs. the control or health group. The results are expressed as mean±standard deviation (SD) for at least three replicates. GAPDH: glyceraldehyde-3-phosphate dehydrogenase; NRF2: nuclear factor erythroid 2-related factor 2.

intensity of the NRF2 protein in the LPS treatment group and the average fluorescence intensity in the cytoplasm and nucleus decreased.

Simultaneously, cell fractionation (Figs. 3q and 3r) showed that NRF2 expression decreased in the cytoplasm and nucleus, suggesting that LPS negatively

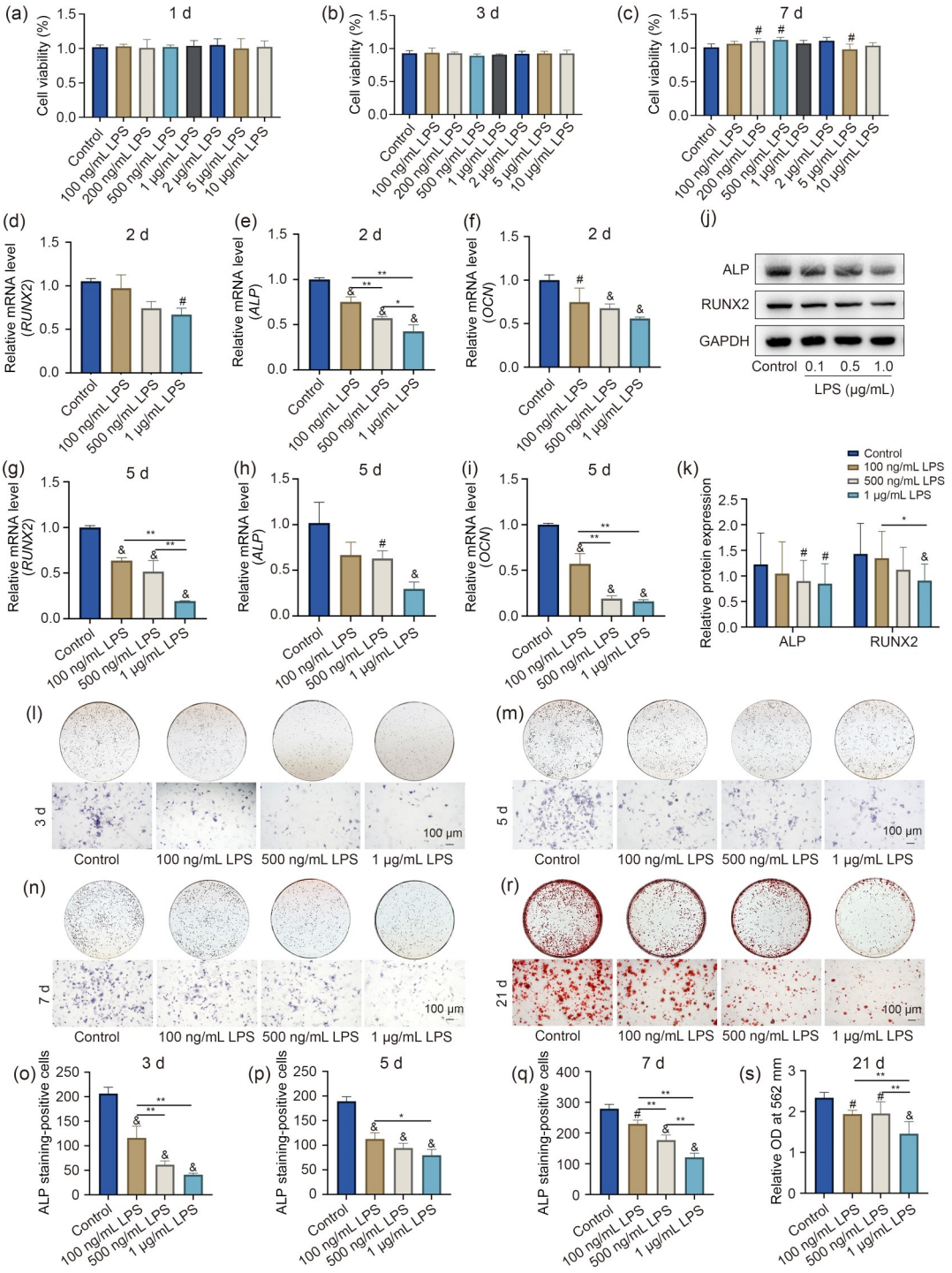

Fig. 2 Inhibition of osteogenic differentiation and mineralization by *Pg*-LPS. (a–c) Cell viability was determined using CCK-8. (d–i) RT-qPCR results for mRNA quantity relative to osteogenesis-related genes at 2 and 5 d. (j, k) Protein expression of osteogenesis-related genes detected by western blotting. (l–q) ALP staining and quantitative evaluation at 3, 5, and 7 d. (r, s) Alizarin red S staining and quantitative evaluation of the mineralized nodules. $^{*}P$<0.05, $^{**}P$<0.01; $^{\#}P$<0.05, $^{\&}P$<0.01 vs. the control group. The results are expressed as mean±standard deviation (SD) for at least three replicates. ALP: alkaline phosphatase; CCK-8: cell counting kit-8; GAPDH: glyceraldehyde-3-phosphate dehydrogenase; LPS: lipopolysaccharide; OCN: osteocalcin; OD: optical density; mRNA: messenger RNA; *Pg*-LPS: *Porphyromonas gingivalis* lipopolysaccharide; RT-qPCR: quantitative reverse transcription-polymerase chain reaction; RUNX2: Runt-related transcription factor 2.

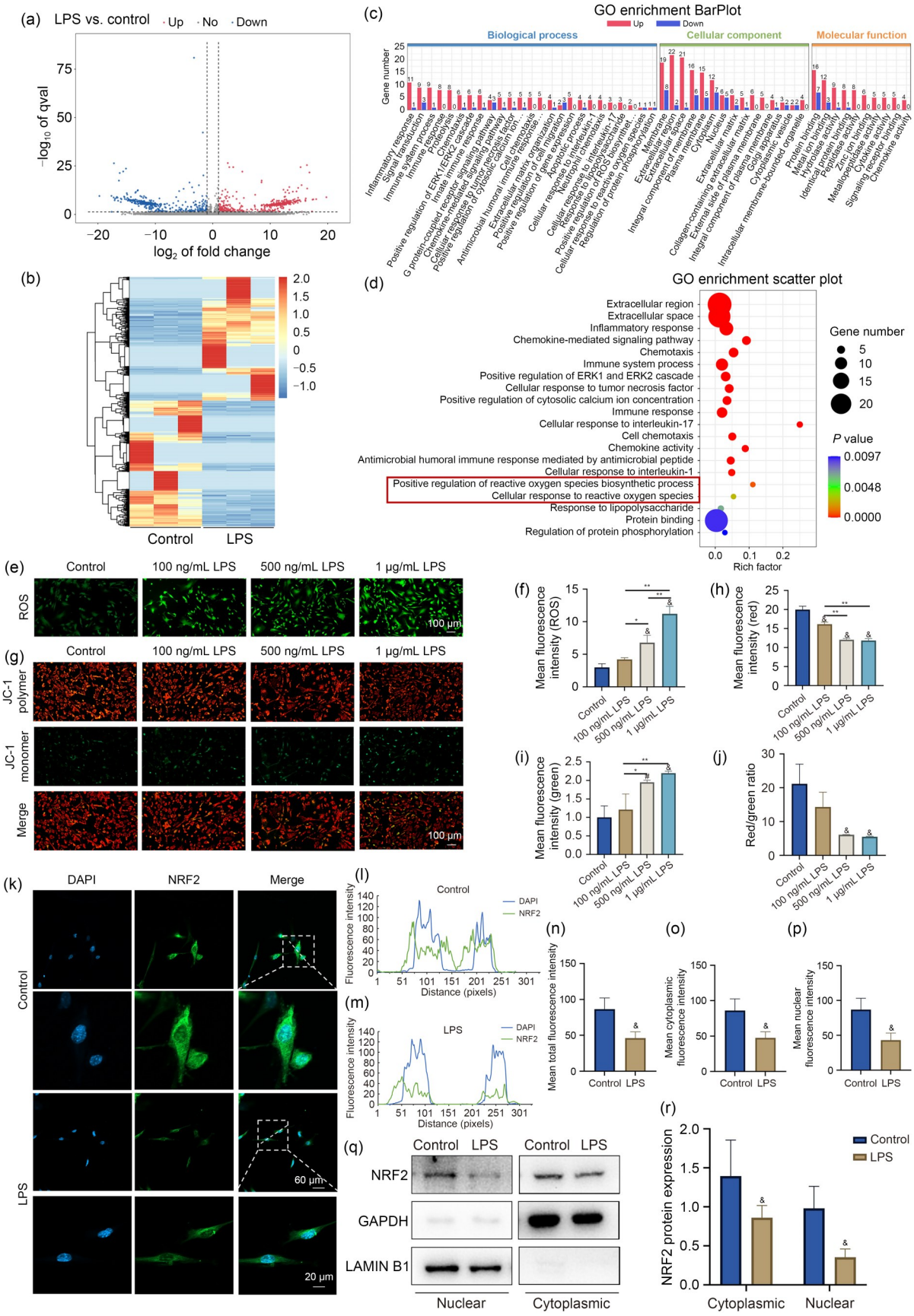
(a) LPS vs. control Up No Down
−log10 of qval
log2 of fold change
(b)
Control LPS
(c) GO enrichment BarPlot
Up Down
Biological process
Cellular component
Molecular function
Gene number
(d) GO enrichment scatter plot
Extracellular region
Extracellular space
Inflammatory response
Chemokine-mediated signaling pathway
Chemotaxis
Immune system process
Positive regulation of ERK1 and ERK2 cascade
Cellular response to tumor necrosis factor
Positive regulation of cytosolic calcium ion concentration
Immune response
Cellular response to interleukin-17
Cell chemotaxis
Chemokine activity
Antimicrobial humoral immune response mediated by antimicrobial peptide
Cellular response to interleukin-1
Positive regulation of reactive oxygen species biosynthetic process
Cellular response to reactive oxygen species
Response to lipopolysaccharide
Protein binding
Regulation of protein phosphorylation
Gene number
P value
Rich factor
(e) Control 100 ng/mL LPS 500 ng/mL LPS 1 μg/mL LPS
ROS
100 μm
(g) Control 100 ng/mL LPS 500 ng/mL LPS 1 μg/mL LPS
JC-1 polymer
JC-1 monomer
Merge
100 μm
(f) Mean fluorescence intensity (ROS)
(h) Mean fluorescence intensity (red)
(i) Mean fluorescence intensity (green)
(j) Red/green ratio
Control
100 ng/mL LPS
500 ng/mL LPS
1 μg/mL LPS
(k) DAPI NRF2 Merge
Control
LPS
60 μm
20 μm
(l) Control
(m) LPS
DAPI
NRF2
Fluorescence intensity
Distance (pixels)
(n) Mean total fluorescence intensity
(o) Mean cytoplasmic fluorescence intensity
(p) Mean nuclear fluorescence intensity
Control LPS
(q) Control LPS Control LPS
NRF2
GAPDH
LAMIN B1
Nuclear
Cytoplasmic
(r) NRF2 protein expression
Control
LPS
Cytoplasmic
Nuclear

Fig. 3 Oxidative stress level, NRF2 expression, and nuclear translocation with *Pg*-LPS treatment. (a) Volcano map of the overall distribution of differentially expressed genes (red: upregulated significantly; blue: downregulated significantly; gray: non-significantly differentially expressed). (b) Heatmap of differentially expressed genes between the LPS and control groups. (c, d) Gene Ontology (GO) enrichment analysis results. (e, f) ROS detection at the intracellular levels. (g–j) JC-1 staining used to observe the mitochondrial membrane potential. (k–p) Microscopy images of NRF2 protein expression. The mean fluorescence intensity was measured. (q, r) Nuclear and cytoplasmic proteins were extracted to detect NRF2 changes. $^{*}P<0.05$, $^{**}P<0.01$; $^{\#}P<0.05$, $^{\&}P<0.01$ vs. the control group. The results are expressed as mean±standard deviation (SD) for at least three replicates. DAPI: 4',6-diamidino-2-phenylindole; GAPDH: glyceraldehyde-3-phosphate dehydrogenase; JC-1: 5,5',6,6'-tetrachloro-1,1',3,3'-tetraethylbenzimidazolylcarbocyanine iodide; *Pg*-LPS: *Porphyromonas gingivalis* lipopolysaccharide; NRF2: nuclear factor erythroid 2-related factor 2; qval: *Q*-value; ROS: reactive oxygen species.

affected cytoplasmic NRF2 expression and nuclear translocation.

3.5 NRF2 expression, oxidative stress, osteogenesis, and mineralization

We determined intracellular ROS levels (Figs. 4a and 4b). The fluorescence intensity increased with NRF2 inhibitor treatment (50 nmol/L brusatol+1 μg/mL LPS), indicating increased ROS and oxidative stress levels. In contrast, fluorescence intensity decreased in the activator group (10 μmol/L TBHQ+1 μg/mL LPS), suggesting decreased ROS and oxidative stress levels.

JC-1 staining was used to detect the MMP in different cell groups (Figs. 4c–4f). The fluorescence intensity and MMP of mandibular osteoblasts decreased significantly in the NRF2 inhibitor group and increased in the activator group.

The ALP expression and mineralized nodule formation decreased in the NRF2 inhibitor group (Figs. 4g–4j). Hence, the inhibition of NRF2 expression reduced the osteogenic differentiation and mineralization ability of cells. NRF2 activators improved the osteogenic differentiation and mineralization of cells.

RT-qPCR (Figs. 4k–4m) and western blot (Figs. 4n and 4o) results confirmed that the mRNA and protein levels of the osteogenic genes were downregulated to different degrees by NRF2 inhibition. The NRF2-activated group showed the opposite results.

3.6 Roles of NRF2 in regulating DUSP1 expression and MAPK pathway

After 3 d of treatment with *Pg*-LPS combined with an NRF2 inhibitor/activator, the expression of DUSP1 consistently decreased with decreasing NRF2 expression and increased with increasing NRF2 expression (Figs. 5a and 5d). NRF2 inhibitors downregulated NRF2 and DUSP1 expression and inhibited the dephosphorylation of the MAPK pathway, whereas NRF2 activators exhibited opposing effects.

Treatment with NRF2 siRNA+LPS had the same effect on the expression of the DUSP1 and MAPK pathway proteins as that observed for the NRF2 inhibitor treatment (Figs. 5b and 5e). NRF2 overexpression had the same effect on the DUSP1 and MAPK pathway protein expression as that observed for NRF2 activator treatment (Figs. 5c and 5f).

3.7 Interaction between NRF2 and DUSP1

The cytoplasmic expression and nuclear translocation of NRF2 decreased in osteoblasts treated with LPS. DUSP1 expression in the cytoplasm and nucleus decreased with the reduction of NRF2 (Figs. 5g–5i).

Immunofluorescence analysis (Fig. 5j) was used to determine whether NRF2 and DUSP1 co-localize in cells, and Co-IP confirmed their physical interaction. Under LPS stimulation, the fluorescence intensities of NRF2 and DUSP1 decreased (Figs. 5k–5o), and the fluorescence changes in the nucleus and cytoplasm were consistent. The Co-IP results (Fig. 5p) indicated that NRF2 could bind to DUSP1 to form a complex.

4 Discussion

The resorption of alveolar bone in periodontitis results in an imbalance of bone homeostasis between osteoblasts and osteoclasts (Bu et al., 2021). Osteogenesis inhibition accelerates the resorption of alveolar bone and promotes the progression of periodontitis. Periodontitis exhibits several complex biological reactions, including anti-infection effects, immune inflammatory responses, and oxidative stress imbalance (Yost et al., 2015; Bunpeng et al., 2022). Excess free radicals and reduced host antioxidant status contribute to the pathogenesis and progression of chronic periodontitis (Sczepanik et al., 2020). This study evaluated the relationship between NRF2 and DUSP1 in the *Pg*-LPS environment and the impact of these factors on osteogenic

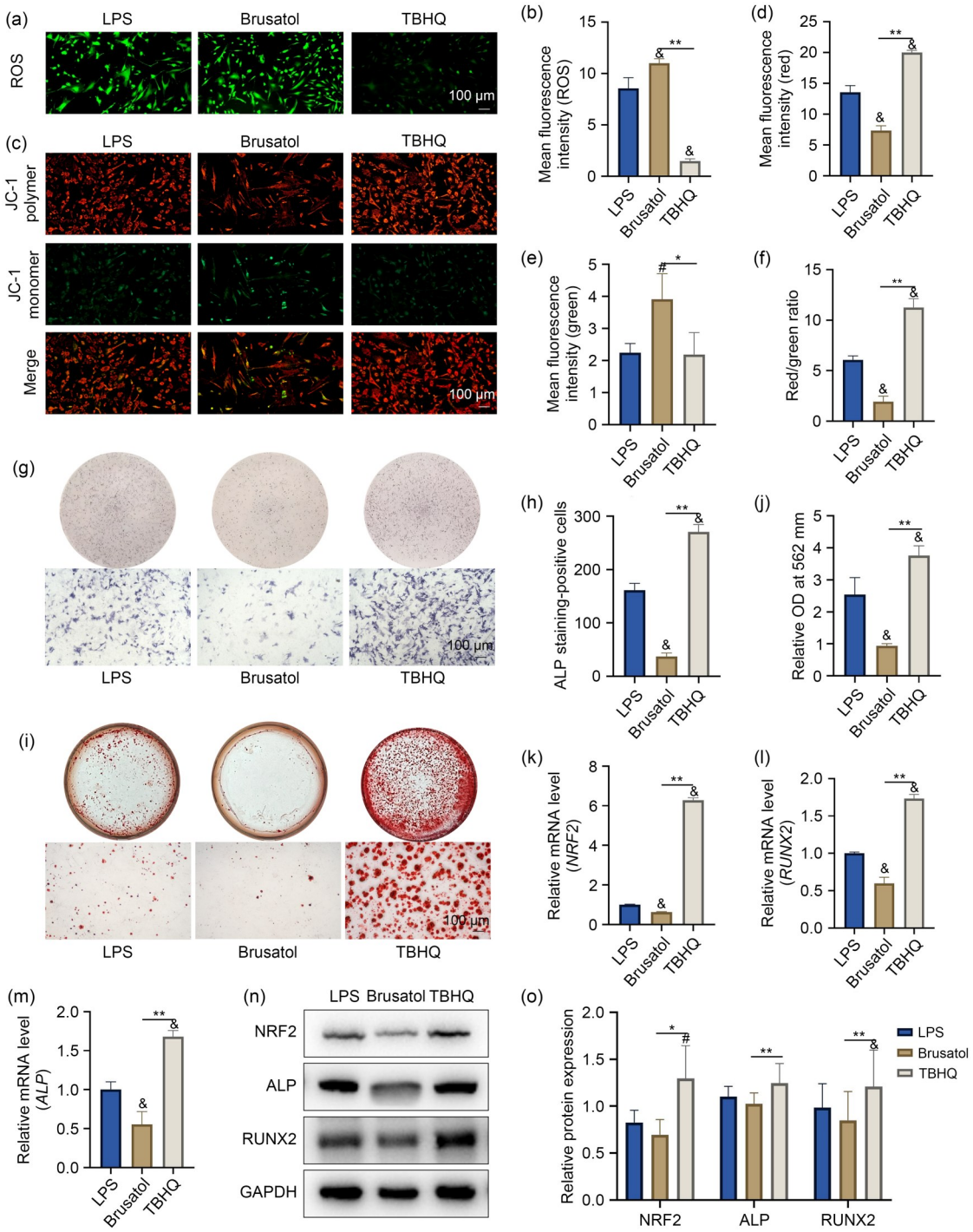

Fig. 4 Relations between NRF2 expression and oxidative stress and osteogenic differentiation. The cells were treated with *Pg*-LPS combined with NRF2 inhibitor or activator. (a, b) Reactive staining was used to detect ROS levels. (c–f) Changes in the mitochondrial membrane potential were measured using JC-1 staining. (g, h) ALP staining. (i, j) Alizarin red S staining. (k–m) RT-qPCR results showing the mRNA levels of osteogenic genes. (n, o) Western blotting analysis of the protein expression of osteoblast-related genes. $^{*}P<0.05$, $^{**}P<0.01$; $^{\#}P<0.05$, $^{\&}P<0.01$ vs. the LPS group. The results are expressed as mean±standard deviation (SD) for at least three replicates. ALP: alkaline phosphatase; OD: optical density; GAPDH: glyceraldehyde-3-phosphate dehydrogenase; JC-1: 5,5',6,6'-tetrachloro-1,1',3,3'-tetraethylbenzimidazolylcarbocyanine iodide; mRNA: messenger RNA; NRF2: nuclear factor erythroid 2-related factor 2; *Pg*-LPS: *Porphyromonas gingivalis* lipopolysaccharide; ROS: reactive oxygen species; RT-qPCR: quantitative reverse transcription-polymerase chain reaction; RUNX2: Runt-related transcription factor 2; TBHQ: tert-butylhydroquinone.

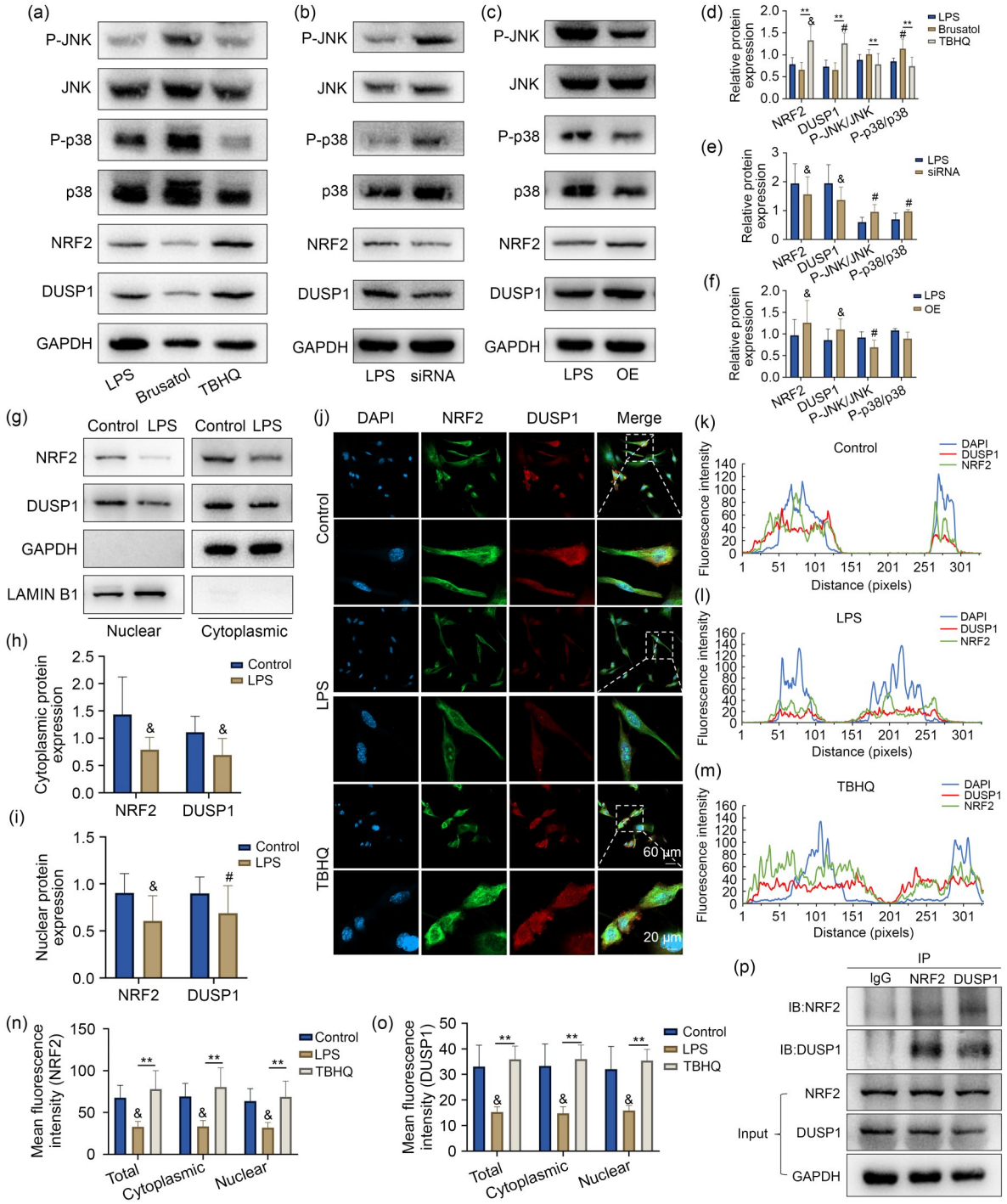

Fig. 5 Effects of NRF2 expression on DUSP1 expression and MAPK pathway. (a, d) Cells were treated with *Pg*-LPS combined with NRF2 inhibitor/activator. (b, e) Cells were transfected with siNRF2. (c, f) Cells were transfected with overexpressed (OE) NRF2. (g–i) NRF2 and DUSP1 expression in nuclear and cytoplasmic proteins. (j) Immunofluorescence colocalization of NRF2 (green) and DUSP1 (red). (k–o) Mean fluorescence intensity of NRF2 and DUSP1. (p) Interaction between NRF2 and DUSP1 was determined using Co-IP. $^{*}P<0.05$, $^{**}P<0.01$; $^{\#}P<0.05$, $^{\&}P<0.01$ vs. the LPS (d–f) or control (h, i, n, o) group. The results are expressed as mean±standard deviation (SD) for at least three replicates. DAPI: 4',6-diamidino-2-phenylindole; DUSP1: dual-specific phosphatase 1; GAPDH: glyceraldehyde-3-phosphate dehydrogenase; IB: immunoblotting; IP: immunoprecipitation; JNK: c-Jun N-terminal kinase; MAPK: mitogen-activated protein kinase; NRF2: nuclear factor erythroid 2-related factor 2; P: phosphorylated; siNRF2: small interfering RNA (siRNA) NRF2; *Pg*-LPS: *Porphyromonas gingivalis* lipopolysaccharide; TBHQ: tert-butylhydroquinone.

differentiation (Fig. 6). The results show that LPS inhibits osteogenic differentiation and that the upregulation of NRF2 expression improves this inhibitory effect. To the best of our knowledge, this is the first study to demonstrate an association between NRF2 and DUSP1 expression in an inflammatory environment that simulates periodontitis. We demonstrated a protein interaction between NRF2 and DUSP1, which may regulate osteogenic differentiation. However, their binding sites are unclear, and whether they interact directly or indirectly should be explored in future studies. Additionally, we must acknowledge that we did not investigate the impact of *Pg*-LPS on osteoclasts, which is a limitation of this study.

We constructed a model based on previous experimental periodontitis murine models by 5-0 ligation of the bilateral maxillary second molars and local injection of *Pg*-LPS to mimic the pathogenic factors of periodontitis (Abe and Hajishengallis, 2013; Li et al., 2020; Ma et al., 2023). We aimed to explore the expression of NRF2 in healthy and periodontitis tissues. We observed alveolar bone resorption in the periodontitis group, suggesting that the model was successfully constructed and that LPS may promote bone resorption and inhibit bone regeneration (Bhattarai et al., 2016). Furthermore, section images demonstrated that experimental periodontitis models presented lower NRF2 protein expression, compared to healthy periodontal models. We observed the downregulation of NRF2 expression in periodontitis tissue samples. Similarly, studies consistently show that NRF2 expression is downregulated in periodontitis model rats (Bhattarai et al., 2016; Li XM et al., 2018; Zhu et al., 2020). Moreover, Gou et al. (2022) observed decreased NRF2 levels in periodontal tissues of individuals with periodontitis. Kasnak et al. (2018) found no significant NRF2 variation among periodontitis patients, which could be attributed to individual differences or uncontrollable factors.

The effects of *Pg*-LPS on osteogenesis and NRF2 expression in mandibular osteoblasts were studied in vitro. *Pg*-LPS inhibited the differentiation and mineralization of osteoblasts, which is consistent with previous findings (Zhou et al., 2021; Guo and Li, 2022). Kadono et al. (1999) proposed that *Pg*-LPS inhibits ALP activity and calcium nodule production in primary mouse osteoblasts. Similarly, under LPS stimulation, the expression of osteogenic markers such as RUNX2, ALP, and OCN was reduced in bone marrow-derived mesenchymal stem cells (BMSCs) (Zhou et al.,

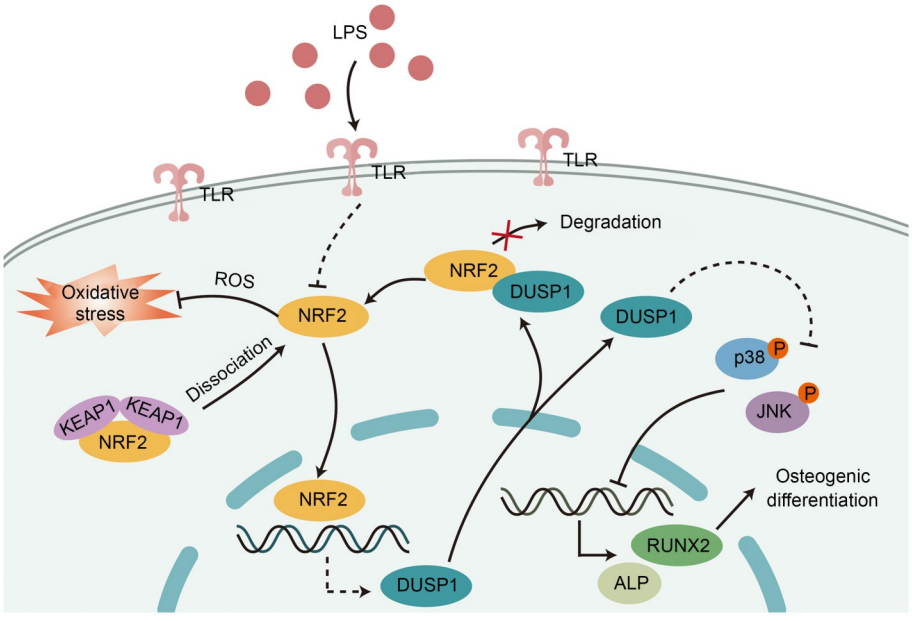

Fig. 6 Schematic illustration of the proposed mechanisms by which NRF2 could regulate DUSP1 to influence osteogenic differentiation. "→" represents promoting effects; "⊣" represents the inhibitory effect. Solid lines indicate relationships confirmed by existing literature, whereas dashed lines denote those experimentally validated in this study. ALP: alkaline phosphatase; DUSP1: dual-specific phosphatase 1; JNK: c-Jun N-terminal kinase; KEAP1: Kelch-like ECH-associated protein 1; LPS: lipopolysaccharide; NRF2: nuclear factor erythroid-2-related factor 2; P: phosphorylation; ROS: reactive oxygen species; RUNX2: Runt-related transcription factor 2; TLR: Toll-like receptor.

2021) and human periodontal ligament stem cells (hPDLSCs) (Guo and Li, 2022). LPS-induced inflammation inhibited the activity of ALP and the expression of osteogenic markers, including OCN and RUNX2. *Pg*-LPS promoted the accumulation of ROS and downregulated the MMP expression in mandibular osteoblasts. These results demonstrate that LPS may induce ROS accumulation, mitochondrial depolarization, and membrane potential reduction in osteoblasts, indicating the imbalance of cellular oxidative stress. This finding is consistent with previous studies showing that ROS levels increase when *Pg*-LPS stimulated HGFs (Liu et al., 2023) and TNF-α stimulated hPDLCs (Fang et al., 2020). Subsequently, we found that the increase in ROS levels after LPS treatment was accompanied by a decrease in NRF2 expression, which is consistent with the findings of previous studies. Zhu et al. (2020) reported that the mRNA level of *NFE2L2* was significantly reduced in LPS-treated hGECs.

NRF2 is an antioxidant regulator of cellular oxidative stress and may be closely associated with the onset and development of periodontitis (Li XM et al., 2018). The nuclear translocation of NRF2 can regulate antioxidant response element (ARE)-dependent genes involved in oxidation and oxidative signaling management, as well as in autophagy, inflammasomes, and mitochondrial biogenesis (Ma, 2013). *Pg*-LPS inhibits NRF2 by diminishing its overall protein level and potentially by impeding its nuclear translocation, thereby preventing it from activating AREs to drive gene transcription. Herein, changes in cellular oxidative stress levels, including ROS levels and MMP values, manifested when NRF2 expression and nuclear translocation were decreased or increased. After downregulating the expression of ROS-related gene cyclophilin D (*CypD*) in MC3T3-E1 osteoblast cells, the expression of the osteogenesis markers RUNX2 and ALP increased (Gan et al., 2018).

Our results suggested that the osteogenic differentiation ability of osteoblasts was inhibited when NRF2 and its nuclear translocation were inhibited. Conversely, osteogenic differentiation was enhanced when NRF2 was activated. Both the osteogenic differentiation and mineralization of cells were inhibited by a decrease in NRF2 expression and nuclear translocation, and vice versa with NRF2 activation. NRF2 and its nuclear translocation have been linked with osteogenic reactions. In ovariectomized murine models with an *Nfe2l2* knockout, nuclear translocation of NRF2 was lost, and OCN secretion bone mineral density was reduced (Chen et al., 2021). The expression of osteocyte genes was reduced when NRF2 was knocked out and was enhanced in osteocytes overexpressing NRF2 (Sánchez-de-Diego et al., 2021). Chung et al. (2014) proposed that *Nfe2l2* siRNA preconditioning during the differentiation of periodontal membrane cells into osteoblasts could block the differentiation of osteoblasts stimulated by deferoxamine (DFO). Wang YF et al. (2022) employed salidroside to enhance the expression of NRF2 and promote its nuclear translocation, resulting in the promotion of osteogenic markers in osteoblasts and the mitigation of osteoporosis in ovariectomized mice.

MAPK is the basic mediator of osteoblast function; p38 MAPK is indispensable in bone development (Greenblatt et al., 2010), and ERK and p38 MAPKs promote the phosphorylation of RUNX2 to regulate osteogenic differentiation (Greenblatt et al., 2013; Wu et al., 2016). Our findings suggested that DUSP1 (which modulates the MAPK signaling pathway) expression was restrained and the phosphorylation of JNK and p38 was enhanced when NRF2 was knocked down, indicating that NRF2 overexpression promotes osteogenic differentiation by way of the MAPK signaling pathway. Immunolocalization and Co-IP analyses confirmed that NRF2 and DUSP1 physically interact in cells, implying that NRF2 and DUSP1 may positively influence cellular antioxidant activity and osteogenic differentiation. Previous studies on lung adenocarcinoma cells have shown that NRF2 and DUSP1 bind to each other to form a positive feedback loop in lung cancer cells, which stabilizes and activates NRF2, thereby promoting anabolic and glutathione (GSH) biosynthesis (Wang et al., 2019). Luo et al. (2018) identified a positive feedback loop between DUSP1 and NRF2, where DUSP1 enhances NRF2 activity by interacting with its NEH2 domain. NRF2 increases *DUSP1* mRNA expression by binding to the ARE site at −1719 to −1710 bp in the promoter. Li J et al. (2018) similarly verified the direct binding interaction between DUSP1 and NRF2.

Takahashi (2011) revealed that the forced expression of exogenous MKP-1 in 3T3-L1 cells resulted in a pronounced accumulation of matrix mineralization, accompanied by the induction of ALP activity. Given the pivotal role of DUSP1 in the MAPK pathway, it is plausible to hypothesize that DUSP1 may exert either direct or indirect influence on RUNX2 and ALP. However, further investigation is required to determine

whether this regulation is dependent on pathways other than the MAPK pathway. Furthermore, KEAP1 typically serves to inhibit NRF2 by mediating its ubiquitination and subsequent degradation in the cytoplasm. However, the specific mechanism underlying KEAP1 and NRF2 in response to *Pg*-LPS warrants further investigation.

In summary, our study revealed that *Pg*-LPS reduced NRF2 expression in the cytoplasm and nucleus of osteoblasts and inhibited osteogenic differentiation and bone formation. A decrease in NRF2 nuclear translocation may inhibit the formation of complexes between NRF2 and DUSP1 and may participate in the dephosphorylation of MAPK pathway proteins. While the binding between NRF2 and DUSP1 has been proved, further studies are needed on NRF2- and DUSP1-binding sites and modes. This study may help determine the relationships between NRF2, DUSP1, and osteogenic differentiation and provide new avenues for periodontitis treatment.

Data availability statement

All statistical data supporting the findings of this study are available within the paper.

Acknowledgments

This work was supported by the National Natural Science Foundation of China (Nos. 82170954 and 82301066), the Medical Science and Technology Project of Zhejiang Province of China (No. 2024KY1064), and the Zhejiang Provincial Natural Science Foundation of China (No. LQN25H140005). We are grateful for the technical support provided by Jingyao CHEN and Chao BI of Core Facilities, Zhejiang University School of Medicine, Hangzhou, China.

Author contributions

All authors have made substantial contributions to the study. Xufei YU, Zhongxiu WANG, and Lili CHEN designed the experiments. Xufei YU, Jiaqi BAO, and Wenlin YUAN performed the research. Xufei YU, Yingming WEI, and Yuting YANG analyzed the data. Xufei YU and Zhongxiu WANG wrote the manuscript. Xufei YU, Jiaqi BAO, and Zhongxiu WANG revised the manuscript. All authors have read and approved the final manuscript, and therefore, have full access to all the data in the study and take responsibility for the integrity and security of the data.

Compliance with ethics guidelines

Xufei YU, Jiaqi BAO, Yingming WEI, Yuting YANG, Wenlin YUAN, Lili CHEN, and Zhongxiu WANG declare that they have no conflicts of interest.

This study was approved by the Institutional Ethics Review Board of The Second Affiliated Hospital of Zhejiang University School of Medicine (Approval Nos. 2021-1078 and 2024-115). Animal experimental protocols were performed according to the ethical requirements and the Guide for the Care and Use of Laboratory Animals, 8th edition (National Research Council, 2011).

References

Abe T, Hajishengallis G, 2013. Optimization of the ligature-induced periodontitis model in mice. *J Immunol Methods*, 394(1-2):49-54. https://doi.org/10.1016/j.jim.2013.05.002

Baird L, Swift S, Llères D, et al., 2014. Monitoring Keap1–Nrf2 interactions in single live cells. *Biotechnol Adv*, 32(6): 1133-1144. https://doi.org/10.1016/j.biotechadv.2014.03.004

Bhattarai G, Poudel SB, Kook SH, et al., 2016. Resveratrol prevents alveolar bone loss in an experimental rat model of periodontitis. *Acta Biomater*, 29:398-408. https://doi.org/10.1016/j.actbio.2015.10.031

Bu TT, Zheng JX, Liu L, et al., 2021. Milk proteins and their derived peptides on bone health: biological functions, mechanisms, and prospects. *Compr Rev Food Sci Food Saf*, 20(2):2234-2262. https://doi.org/10.1111/1541-4337.12707

Bunpeng N, Boriboonhirunsarn D, Boriboonhirunsarn C, et al., 2022. Association between gestational diabetes mellitus and periodontitis via the effect of reactive oxygen species in peripheral blood cells. *J Periodontol*, 93(5):758-769. https://doi.org/10.1002/JPER.21-0455

Chen CT, Shih YRV, Kuo TK, et al., 2008. Coordinated changes of mitochondrial biogenesis and antioxidant enzymes during osteogenic differentiation of human mesenchymal stem cells. *Stem Cells*, 26(4):960-968. https://doi.org/10.1634/stemcells.2007-0509

Chen XR, Zhu XB, Wei A, et al., 2021. Nrf2 epigenetic derepression induced by running exercise protects against osteoporosis. *Bone Res*, 9:15. https://doi.org/10.1038/s41413-020-00128-8

Chung JH, Kim YS, Noh K, et al., 2014. Deferoxamine promotes osteoblastic differentiation in human periodontal ligament cells via the nuclear factor erythroid 2-related factor-mediated antioxidant signaling pathway. *J Periodontal Res*, 49(5):563-573. https://doi.org/10.1111/jre.12136

Fang H, Yang K, Tang P, et al., 2020. Glycosylation end products mediate damage and apoptosis of periodontal ligament stem cells induced by the JNK-mitochondrial pathway. *Aging*, 12(13):12850-12868. https://doi.org/10.18632/aging.103304

Fiedler T, Salamon A, Adam S, et al., 2013. Impact of bacteria and bacterial components on osteogenic and adipogenic differentiation of adipose-derived mesenchymal stem cells.

Exp Cell Res, 319(18):2883-2892. https://doi.org/10.1016/j.yexcr.2013.08.020

Fu XH, Chen CZ, Li S, et al., 2019. Dual-specificity phosphatase 1 regulates cell cycle progression and apoptosis in cumulus cells by affecting mitochondrial function, oxidative stress, and autophagy. *Am J Physiol Cell Physiol*, 317(6):C1183-C1193. https://doi.org/10.1152/ajpcell.00012.2019

Gan XQ, Zhang L, Liu BL, et al., 2018. CypD-mPTP axis regulates mitochondrial functions contributing to osteogenic dysfunction of MC3T3-E1 cells in inflammation. *J Physiol Biochem*, 74(3):395-402. https://doi.org/10.1007/s13105-018-0627-z

Gou HQ, Chen X, Zhu XM, et al., 2022. Sequestered SQSTM1/p62 crosstalk with Keap1/NRF2 axis in hPDLCs promotes oxidative stress injury induced by periodontitis. *Free Radical Biol Med*, 190:62-74. https://doi.org/10.1016/j.freeradbiomed.2022.08.001

Greenblatt MB, Shim JH, Zou WG, et al., 2010. The p38 MAPK pathway is essential for skeletogenesis and bone homeostasis in mice. *J Clin Invest*, 120(7):2457-2473. https://doi.org/10.1172/JCI42285

Greenblatt MB, Shim JH, Glimcher LH, 2013. Mitogen-activated protein kinase pathways in osteoblasts. *Annu Rev Cell Dev Biol*, 29:63-79. https://doi.org/10.1146/annurev-cellbio-101512-122347

Guo L, Li L, 2022. LIN28A alleviates inflammation, oxidative stress, osteogenic differentiation and mineralization in lipopolysaccharide (LPS)-treated human periodontal ligament stem cells. *Exp Ther Med*, 23(6):411. https://doi.org/10.3892/etm.2022.11338

Herzmann N, Salamon A, Fiedler T, et al., 2017. Lipopolysaccharide induces proliferation and osteogenic differentiation of adipose-derived mesenchymal stromal cells in vitro via TLR4 activation. *Exp Cell Res*, 350(1):115-122. https://doi.org/10.1016/j.yexcr.2016.11.012

Kadono H, Kido JI, Kataoka M, et al., 1999. Inhibition of osteoblastic cell differentiation by lipopolysaccharide extract from *Porphyromonas gingivalis*. *Infect Immun*, 67(6):2841-2846. https://doi.org/10.1128/IAI.67.6.2841-2846.1999

Kasnak G, Firatli E, Könönen E, et al., 2018. Elevated levels of 8-OHdG and PARK7/DJ-1 in peri-implantitis mucosa. *Clin Implant Dent Relat Res*, 20(4):574-582. https://doi.org/10.1111/cid.12619

Kim JM, Yang YS, Park KH, et al., 2019. The ERK MAPK pathway is essential for skeletal development and homeostasis. *Int J Mol Sci*, 20(8):1803. https://doi.org/10.3390/ijms20081803

Kim JM, Lin CJ, Stavre Z, et al., 2020. Osteoblast-osteoclast communication and bone homeostasis. *Cells*, 9(9):2073. https://doi.org/10.3390/cells9092073

Knudsen NØ, Andersen SD, Lützen A, et al., 2009. Nuclear translocation contributes to regulation of DNA excision repair activities. *DNA Repair*, 8(6):682-689. https://doi.org/10.1016/j.dnarep.2009.03.005

Konopka T, Król K, Kopeć W, et al., 2007. Total antioxidant status and 8-hydroxy-2'-deoxyguanosine levels in gingival and peripheral blood of periodontitis patients. *Arch Immunol Ther Exp*, 55(6):417-425. https://doi.org/10.1007/s00005-007-0047-1

Li H, Deng YJ, Tan MM, et al., 2020. Low-intensity pulsed ultrasound upregulates osteogenesis under inflammatory conditions in periodontal ligament stem cells through unfolded protein response. *Stem Cell Res Ther*, 11:215. https://doi.org/10.1186/s13287-020-01732-5

Li J, Wang HY, Zheng ZH, et al., 2018. Mkp-1 cross-talks with Nrf2/Ho-1 pathway protecting against intestinal inflammation. *Free Radical Biol Med*, 124:541-549. https://doi.org/10.1016/j.freeradbiomed.2018.07.002

Li XM, Sun XY, Zhang XR, et al., 2018. Enhanced oxidative damage and Nrf2 downregulation contribute to the aggravation of periodontitis by diabetes mellitus. *Oxid Med Cell Longev*, 2018:9421019. https://doi.org/10.1155/2018/9421019

Liu J, Wang XX, Zheng M, et al., 2023. Oxidative stress in human gingival fibroblasts from periodontitis versus healthy counterparts. *Oral Dis*, 29(3):1214-1225. https://doi.org/10.1111/odi.14103

Liu SY, Yang LY, Mu S, et al., 2018. Epigallocatechin-3-gallate ameliorates glucocorticoid-induced osteoporosis of rats *in vivo* and *in vitro*. *Front Pharmacol*, 9:447. https://doi.org/10.3389/fphar.2018.00447

Loos BG, van Dyke TE, 2020. The role of inflammation and genetics in periodontal disease. *Periodontol 2000*, 83(1):26-39. https://doi.org/10.1111/prd.12297

Luo L, Chen YR, Wang HY, et al., 2018. Mkp-1 protects mice against toxin-induced liver damage by promoting the Nrf2 cytoprotective response. *Free Radical Biol Med*, 115:361-370. https://doi.org/10.1016/j.freeradbiomed.2017.12.010

Ma Q, 2013. Role of Nrf2 in oxidative stress and toxicity. *Annu Rev Pharmacol Toxicol*, 53:401-426. https://doi.org/10.1146/annurev-pharmtox-011112-140320

Ma XY, Chen X, Duan ZH, et al., 2023. Circadian rhythm disruption exacerbates the progression of macrophage dysfunction and alveolar bone loss in periodontitis. *Int Immunopharmacol*, 116:109796. https://doi.org/10.1016/j.intimp.2023.109796

National Research Council, 2011. Guide for the Care and Use of Laboratory Animals, 8th Ed. The National Academies Press, Washington, USA. https://doi.org/10.17226/12910

Sánchez-de-Diego C, Pedrazza L, Pimenta-Lopes C, et al., 2021. NRF2 function in osteocytes is required for bone homeostasis and drives osteocytic gene expression. *Redox Biol*, 40:101845. https://doi.org/10.1016/j.redox.2020.101845

Sczepanik FSC, Grossi ML, Casati M, et al., 2020. Periodontitis

is an inflammatory disease of oxidative stress: we should treat it that way. *Periodontol 2000*, 84(1):45-68. https://doi.org/10.1111/prd.12342

Sies H, Berndt C, Jones DP, 2017. Oxidative stress. *Annu Rev Biochem*, 86:715-748. https://doi.org/10.1146/annurev-biochem-061516-045037

Silva-Islas CA, Maldonado PD, 2018. Canonical and non-canonical mechanisms of Nrf2 activation. *Pharmacol Res*, 134:92-99. https://doi.org/10.1016/j.phrs.2018.06.013

Su HX, Gornitsky M, Velly AM, et al., 2009. Salivary DNA, lipid, and protein oxidation in nonsmokers with periodontal disease. *Free Radical Biol Med*, 46(7):914-921. https://doi.org/10.1016/j.freeradbiomed.2009.01.008

Sun YX, Li L, Corry KA, et al., 2015. Deletion of Nrf2 reduces skeletal mechanical properties and decreases load-driven bone formation. *Bone*, 74:1-9. https://doi.org/10.1016/j.bone.2014.12.066

Takahashi T, 2011. Overexpression of Runx2 and MKP-1 stimulates transdifferentiation of 3T3-L1 preadipocytes into bone-forming osteoblasts in vitro. *Calcif Tissue Int*, 88(4):336-347. https://doi.org/10.1007/s00223-011-9461-9

Tang X, Ma SH, Li YR, et al., 2020. Evaluating the activity of sodium butyrate to prevent osteoporosis in rats by promoting osteal GSK-3β/Nrf2 signaling and mitochondrial function. *J Agric Food Chem*, 68(24):6588-6603. https://doi.org/10.1021/acs.jafc.0c01820

Wang HY, Liu KH, Chi ZX, et al., 2019. Interplay of MKP-1 and Nrf2 drives tumor growth and drug resistance in non-small cell lung cancer. *Aging*, 11(23):11329-11346. https://doi.org/10.18632/aging.102531

Wang L, Zhang X, Xiong XX, et al., 2022. Nrf2 regulates oxidative stress and its role in cerebral ischemic stroke. *Antioxidants*, 11(12):2377. https://doi.org/10.3390/antiox11122377

Wang YF, Chang YY, Zhang XM, et al., 2022. Salidroside protects against osteoporosis in ovariectomized rats by inhibiting oxidative stress and promoting osteogenesis via Nrf2 activation. *Phytomedicine*, 99:154020. https://doi.org/10.1016/j.phymed.2022.154020

Wu MR, Chen GQ, Li YP, 2016. TGF-β and BMP signaling in osteoblast, skeletal development, and bone formation, homeostasis and disease. *Bone Res*, 4:16009. https://doi.org/10.1038/boneres.2016.9

Xiao J, Han QG, Yu ZC, et al., 2023. Morroniside inhibits inflammatory bone loss through the TRAF6-mediated NF-κB/MAPK signalling pathway. *Pharmaceuticals*, 16(10):1438. https://doi.org/10.3390/ph16101438

Yen CH, Hsu CM, Hsiao SY, et al., 2020. Pathogenic mechanisms of myeloma bone disease and possible roles for NRF2. *Int J Mol Sci*, 21(18):6723. https://doi.org/10.3390/ijms21186723

Yost S, Duran-Pinedo AE, Teles R, et al., 2015. Functional signatures of oral dysbiosis during periodontitis progression revealed by microbial metatranscriptome analysis. *Genome Med*, 7:27. https://doi.org/10.1186/s13073-015-0153-3

Zhou R, Chen FB, Liu HX, et al., 2021. Berberine ameliorates the LPS-induced imbalance of osteogenic and adipogenic differentiation in rat bone marrow-derived mesenchymal stem cells. *Mol Med Rep*, 23(5):350. https://doi.org/10.3892/mmr.2021.11989

Zhu CH, Zhao Y, Wu XY, et al., 2020. The therapeutic role of baicalein in combating experimental periodontitis with diabetes via Nrf2 antioxidant signaling pathway. *J Periodontal Res*, 55(3):381-391. https://doi.org/10.1111/jre.12722

Zhu L, Lin ZW, Wang G, et al., 2019. MicroRNA-495 downregulates AQP1 and facilitates proliferation and differentiation of osteoblasts in mice with tibial fracture through activation of p38 MAPK signaling pathway. *Sci Rep*, 9:16171. https://doi.org/10.1038/s41598-019-50013-6

Supplementary information

Tables S1–S3